Enhanced Laplace Pressures for Functional Surfaces: Wicking, Switchability, and Selectivity

Kyle L. Wilke, Youngsup Song, Zhengmao Lu, and Evelyn N. Wang

Dr. K. L. Wilke, Dr. Y. Song, Dr. Z. Lu, Prof. E. N. Wang
Department of Mechanical Engineering, Massachusetts Institute of Technology, Cambridge, MA 02139, USA
E-mail: enwang@mit.edu

Keywords: reentrant structures, switchable wetting, selective wetting, smart surfaces, hydrophilic/hydrophobic

Wetting functionalities of rough surfaces are largely determined by the Laplace pressure generated across liquid-gas interfaces formed within surface structures. Typically, rough wetting surfaces create negative Laplace pressures, enabling capillary wicking, while rough non-wetting surfaces create positive Laplace pressures, exhibiting fluid repellency. Here, with microfabricated reentrant structures, we show that the same surface can exhibit either a negative or positive Laplace pressure, regardless of its intrinsic wettability. This material-independent Laplace pressure duality enables or enhances a range of wetting functionalities including wicking, switchability, and selectivity. On the same surface, we demonstrate capillary rise, capillary dip, and the combination of the two which leads to further enhancement of the total sustainable capillary height and Laplace pressure, the driving force for wicking. Further, we showed active switching of wetting states between the hemiwicking and the repellent Cassie state on reentrant structures. Moreover, with a water-hexane mixture system, we demonstrated selective wetting of reentrant structures, i.e., water can be selectively wicked or repelled in the presence of hexane, and vice versa. We achieve these functionalities, which would typically require complex chemical coatings, solely using surface structures, thus largely expanding the design space for a wide range of thermofluidic applications.

Functional surfaces that wick liquids or have switchable and selective wettabilities have found utility in a broad range of applications.[1] Wicking is used in a variety of applications including microfluidics,[2] anti-fogging,[3] liquid separation,[4] and heat transfer enhancement via boiling and thin film evaporation.[5] Switchable surfaces that can dynamically tune the surface wettability from repellency to wicking and vice versa (**Figure 1a**) have shown potential in tunable liquid lenses,[6] switchable valves,[7] biosensors,[8] nanomedicine,[9] and microrobots.[10] Surfaces that exhibit selective wetting of one liquid to

the other (Figure 1b), on the other hand, have received attention for separation of liquid mixtures, e.g., oil-water separation.[1a] All these functionalities are based on two extreme wetting states, i.e., repellent (Figure 1c) and wicking states (Figure 1d). The repellent or wicking surfaces are typically obtained by surface roughening, which enhances the intrinsic wetting behavior of smooth surfaces, i.e., wetting surfaces become more wetting (or wicking in the extreme) and non-wetting surfaces become more non-wetting (or repellent in the extreme).[11] The close-up views (Figure 1c-i, d-i) of the liquid meniscus reveal the critical role of Laplace pressure in these extreme wettabilities. The Laplace pressure represents the pressure difference across the liquid-gas interface and can be expressed as $\Delta P_L = \gamma H$, where γ and H are liquid surface tension and mean curvature, respectively. When a liquid drop sits on an intrinsically non-wetting surface ($\theta > 90°$) structured to be repellent (Figure 1c-i), the three-phase contact line pins at the top of the structures, leaving an air layer underneath. In this case, the liquid has higher pressure than air and we define H to be positive, rendering positive ΔP_L. On the other hand, when liquid contacts an intrinsically wetting surface ($\theta < 90°$) structured to be wicking (Figure 1d-i), the liquid has lower pressure than air and we define H to be negative, resulting in negative ΔP_L. Complex functionalities such as switchability and selectivity are, therefore, realized through manipulation of Laplace pressure. The switchability is achieved through the control of the sign of ΔP_L by external stimuli to shift from a repellent to wicking state, and vice-versa. Common switching stimuli include temperature,[12] light,[13] pH,[14] electrical potential,[15] pre-wetting and drying,[16] and mechanical strain,[17] which consequently cause changes in surface geometries or energies. On the other hand, selective wetting of one liquid to the other generally requires a surface that exhibits positive ΔP_L for one liquid and negative ΔP_L for the other. To tailor the sign of ΔP_L for effective separation of oil-water mixtures, for example, various surface treatment methods have been utilized including electrochemical or acidic treatments of metallic surfaces,[18] and

surface coatings with polymers,[4b, 19] silanes,[20] thiols,[21] self-assembled monolayers,[22] and hydrogels.[23]

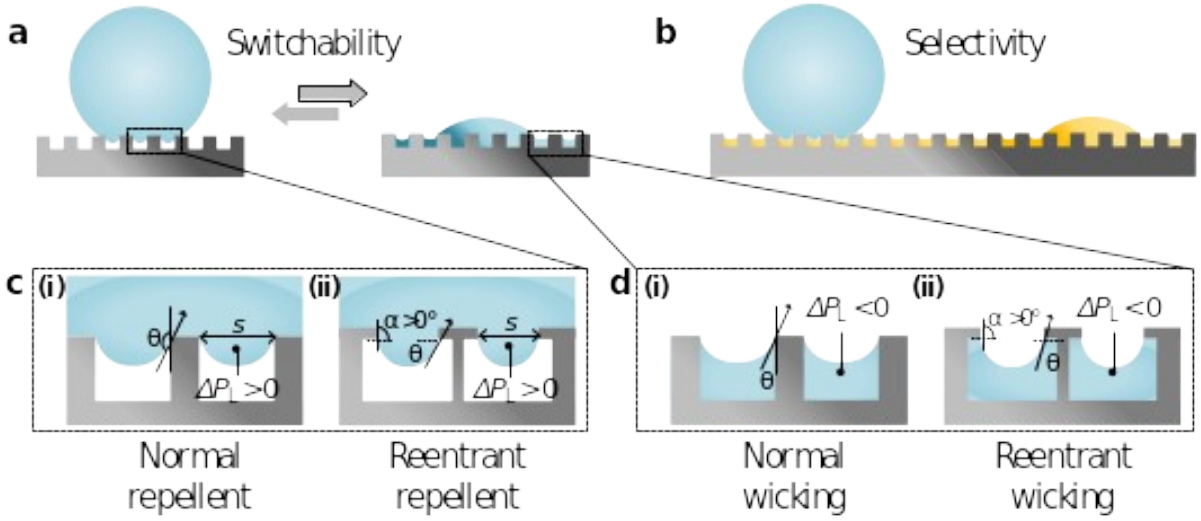

Figure 1. Functional surfaces and the role of Laplace pressure. (a) A switchable surface that can tune its surface wettability from repellency to wicking, and vice versa. (b) A selective surface that has selective wetting of one liquid to the other. (c) Close-up schematic of a liquid meniscus on repellent surfaces: droplets form positive Laplace pressure on a structured, intrinsically non-wetting surface (c-i) and on reentrant structures (c-ii), where reentrant structures can repel an intrinsically wetting liquid ($\theta<90^\circ$). (d) Close-up schematic of a liquid meniscus on hemiwicking surfaces: droplets form negative Laplace pressure on a structured, intrinsically wetting surface (d-i) and on reentrant structures (d-ii), where reentrant structures can wick an intrinsically non-wetting liquid ($\theta>90^\circ$).

Theoretically, with reentrant structures, intrinsically wetting surfaces can exhibit positive ΔP_L (Figure 1c-ii), which has been demonstrated extensively in previous works.[15b, 19a, 24] Recently, we demonstrated non-wetting surfaces can also exhibit negative ΔP_L (Figure 1d-ii) without additional functional coatings, meaning the same surface design can achieve both positive or negative ΔP_L for both wetting or non-wetting liquids.[25] This dual Laplace pressure characteristic of reentrant structures is due to their unique ability to sustain contact line pinning at the reentrant feature. Depending on the reentrance angle, α (Figure 1c-ii and 1d-ii), the surface can repel fluids with different contact angles, θ. The black arrow in the schematics represents the direction of the surface tension force that prevents liquid from

entering the structure. For a non-reentrant microstructure, the surface tension force only acts to prevent liquid entering the microstructure if $\theta > 90°$. The Laplace pressure in this case on micro-channels, for example, is $\Delta P_L = \frac{-2\gamma\cos\theta}{s}$, where s is the spacing between channels (Figure 1c-i). By the addition of reentrance, the direction of the surface tension force is rotated by α to the vertical direction, which enables the surface to repel liquids with contact angles lower than 90° (Figure 1c-ii). At the extreme, for perfectly wetting fluids with $\theta = 0°$, a doubly reentrant microstructure with $\alpha > 90°$ is needed to repel the fluid (see Section S1 of Supporting Information for a description of reentrant and doubly-reentrant surfaces).[24a] Generally in the non-wetting case, reentrant features can increase the Laplace pressure to $\Delta P_L = \frac{-2\gamma\cos(\theta+\alpha)}{s}$. Likewise, reentrant structures may achieve hemiwicking of all liquids when the reentrant structure is initially filled with the same liquid (Figure 1d-ii).[25] In the hemiwicking case, the surface tension force generated at the reentrant structure prevents liquid from being removed from the roughness, where the resulting Laplace pressure is enhanced (to the negative direction) as $\Delta P_L = \frac{-2\gamma\cos(\theta-\alpha)}{s}$. Therefore, a reentrant surface can generate dual Laplace pressure regardless of intrinsic wettability, and the Laplace pressure can be expressed as:

$$\Delta P_L = \frac{-2\gamma\cos(\theta \pm \alpha)}{s} \quad (1)$$

where $\cos(\theta+\alpha)$ is used for the repellent state, i.e., positive ΔP_L, and $\cos(\theta-\alpha)$ is used for the hemiwicking state, i.e., negative ΔP_L. Note that the vertical component of the contact line force reaches the maximum magnitude ($2\gamma/s$) at $\theta + \alpha = 180°$ for the repellent state and $\theta - \alpha = 0°$ for the hemiwicking state. When $\theta + \alpha > 180°$ for the repellent state, the liquid entering the

structure must overcome this $2\gamma/s$ Laplace pressure (Figure S2b). Similarly, when $\theta - \alpha < 0°$, ΔP_L is set to $-2\gamma/s$ for the hemiwicking state.

In this work, we created reentrant microchannels, demonstrated these enhanced Laplace pressures, and further demonstrated switchability and selectivity on the same surface by leveraging the duality of Laplace pressure enabled by reentrant structures. Since previous strategies for switchability and selectivity mostly rely on the intrinsic wettability of a structured surface, the types of liquids associated with the surface are limited.[1] The design flexibility enabled by the dual Laplace pressure of reentrant structures, therefore, can be promising for systems where intrinsic wettability requirements currently limit the design to non-optimal materials and liquids.

To experimentally demonstrate the dual Laplace pressures and resulting functionalities of reentrant structures, we fabricated reentrant microchannels (Figure 2a). The channel width ($d = 90$ μm), height ($H \approx 400$ μm), and pitch ($l = 500$ μm) are the same for both normal and reentrant channels (Figure 2b). The overhangs of reentrant structures have thickness ($t = 1$ μm), length ($D = 25$ μm), and reentrance angle ($\alpha = 90°$). The cross section scanning electron microscope images are shown in Figure 2c. Table S1 summarizes the geometry of tested samples. Before testing, unless otherwise stated, the entire surface was coated with a conformal 60 nm thick, low-surface-energy polymer (C_4F_8) to create a uniform and repeatable contact angle across different tested surfaces, but the coating is not required for the functionalities we demonstrate.

First, we quantified and characterized the dual Laplace pressure by measuring the capillary height of the surface, *h*, which is determined by a balance of the Laplace pressure and the hydrostatic pressure as:

$$h = \frac{2\gamma \cos(\theta \pm \alpha)}{(l-d)\Delta\rho g} \quad (1)$$

where $\Delta\rho$ is the density difference between the liquid and air and g is the gravitational acceleration. $\cos(\theta - \alpha)$ is used for the negative Laplace pressure, i.e., when the surface is hemiwicking (Figure 2e), whereas $\cos(\theta + \alpha)$ is for the positive Laplace pressure, i.e., when the surface is repellent (Figure 2f) (see Section S2 of Supporting Information for a derivation and further explanation). A normalized capillary height, h^*, is then calculated to account for the surface geometry and different properties of liquids used as:

$$h^* = \frac{h(l-d)\Delta\rho g}{2\gamma} = \cos(\theta \pm \alpha) \quad (2)$$

When dipped into a pool of wetting liquid, surfaces with normal channels exhibited hemiwicking, where the liquid rose in the channels a given height as the negative Laplace pressure counteracted gravity. In contrast, when a non-wetting liquid was used, air was trapped within the normal channel surface down to a given depth in the liquid due to the positive Laplace pressure. As a result, a surface without reentrance ($\alpha = 0°$) has a positive capillary height for wetting liquids and a negative capillary height for non-wetting liquids. The black triangles represent the measurement while the dashed line represents the prediction from Equation 2.

Adding reentrance ($\alpha = 90°$) enabled positive (blue squares for measurements and solid blue line for Equation 2) capillary heights for all liquids simply by controlling the initial wetting state. When a reentrant channel prefilled with liquid (the liquid can be either wetting or non-wetting) was raised out of the liquid (Figure 2e and Movie S1, which shows a liquid with $\theta = 91.6°$), liquid remained trapped within the structures to a capillary height exceeding that of normal structures. The liquid started dewetting from the reentrant channels after the maximum sustainable capillary height from Equation 1 was exceeded. This measurement of capillary height demonstrated an important point. The capillary height became much larger compared to normal structures, demonstrating reentrant structures can be used to significantly

enhance Laplace pressure. This enhancement could be leveraged in a variety of applications such as those where enhanced wicking is desired.[5, 26] This enhanced wicking has usually been achieved by changing structure dimensions or using liquids and materials with contact angles close $\theta = 0°$; however, this work demonstrates reentrance can be an important factor as well, particularly for liquids that are not perfectly wetting or even non-wetting, which has not been explored.

Likewise, when a reentrant channel filled with air was lowered into liquid (Figure 2f and Movie S2), air remained trapped within the structures. After the maximum negative capillary height was exceeded, the liquid entered the reentrant structures (red squares in Figure 2d for measurements and solid red line for the prediction from Equation 2). This enhanced repellency enabled by reentrant structures was also reported in previous literature. [19a, 24a]

Furthermore, we showed a filled reentrant channel can increase the sustainable capillary height of the surface by supporting a positive Laplace pressure at one end of the channel and a negative Laplace pressure at the other end simultaneously. In this case, the positive Laplace pressure does not create a repellent surface, but rather prevents liquid within the channels from bursting out of the channel, as depicted in the schematics of Figure 2g. To demonstrate this ability, we conducted another capillary height experiment in which the channels were prefilled, but no pool of liquid was used as in Figure 2e and f. Instead, the capillary height was increased by gradually tilting the prefilled surface starting from horizontal (Figure 2g and Movie S3, in which ethanol was used). The observed capillary height (h enhanced) was the sum of the magnitude of the heights predicted by Equation 1 for the positive (h +) and negative (h -) Laplace pressures. The increase of sustainable capillary height of the surface was further demonstrated for a variety of liquids with a range of intrinsic wettability (purple squares in Figure 2d). Interestingly, the maximum capillary height was not

observed for a perfectly wetting liquid because it cannot sustain any positive Laplace pressure. Rather, liquids with intermediate wettability showed the largest capillary height, where the theoretical maximum occurs for a liquid with a contact angle of 90°. This increase in total Laplace pressure, which is the driving force for wicking, has the potential to impact high performance systems that rely on wicking as discussed above when describing enhanced capillary height.

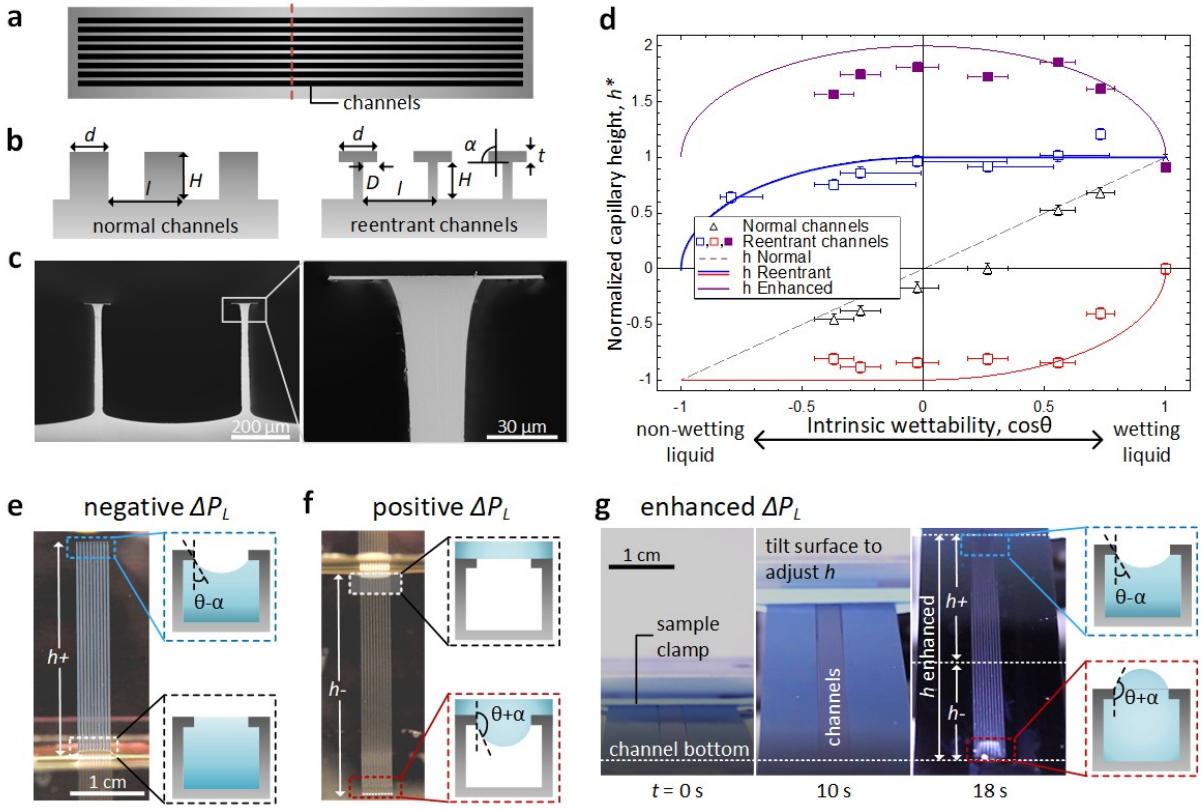

Figure 2. Fabricated microchannels and capillary rise/dip tests. (a) Top-view schematic of the microchannels. (b) Cross-section schematics of the normal channels and the reentrant channels. Width (d = 90 µm) and height ($H \approx 400$ µm) of walls and pitch (l = 500 µm) are the same for both channels. Reentrant channels have overhangs with thickness (t = 1 µm), length (D = 25 µm), and reentrance angle (α = 90°). (c) Cross-section scanning electron microscope images of reentrant channels. (d) Results of capillary rise/dip tests. Normalized capillary height is plotted with respect to function of intrinsic wettability. Normal channels (black triangle) show capillary rise (positive height) for wetting liquids and capillary depression (negative height) for non-wetting liquids. Reentrant channels, on the other hand, can have either capillary rise (blue squares) or depression (red squares) independent of intrinsic wettability. Purple squares show enhanced capillary height resulting from doubled capillary pressures (described in further detail when discussing Figure 2g). The lines are theoretical predictions of normalized capillary heights from Equation 2, which show reasonable agreement with experimental data. (e) Optical image of the capillary rise test. Channels filled

with liquid raised up from the liquid pool. Negative Laplace pressure held the liquids against gravity. (f) Capillary dip test. Channels filled with air dipped into a liquid reservoir. Positive Laplace pressure prevented the liquid from entering the channels. (g) Reentrant channels with positive Laplace pressure at one end and negative Laplace pressure at the other end yielded enhanced capillary height. Initially, the channels prefilled with a liquid was horizontal (t = 0 s). The channels were gradually tilted to increase the capillary height (t = 10 s). The reentrant structures provided positive and negative Laplace pressures at the bottom and the top of the channels, respectively, resulting in enhanced overall capillary height (t = 18 s), resulting in significantly enhanced capillary height as seen in Figure 2d.

By tailoring the dual Laplace pressure of reentrant structures, which is the basis for wicking and repellency, we also demonstrated more complex wetting behaviors like switching and selectivity. First, we demonstrated switching wettability of reentrant structures, which would generally require complex coatings without reentrance features.[12-15] The key is to manipulate the type of fluid, i.e., a liquid or air, inside the reentrant structures, which determines the surface wetting behavior (Figure 3a). Switching from a repellent to wicking state can be achieved simply by filling a liquid into the reentrant channels via a reservoir at the end of the channels. Due to the liquid filled within the channels, liquid contacting the surface exhibited a hemiwicking state with negative ΔP_L. On the other hand, switching from a wicking to repellent state was realized by taking advantage of the gravitational force. As liquid continued to fill the channel, the effective liquid height increased. Once the capillary height was reached, i.e., $L\sin\varphi > h$¿, where L and φ are the channel length and the tilting angle, respectively, liquid was emptied from the channels by gravity; accordingly, the now air-filled reentrant structures became repellent once again due to the resulting positive ΔP_L. We demonstrated active wettability switching in Figure 3b and Movie S4. In this demonstration, droplets added on the surface from a syringe were switched between the repellent state where the droplet rolled down the surface, to a hemiwicking state where the droplet absorbed into the surface. We used a test liquid with an intrinsic advancing contact angle of 91.6°. The surface was tilted to $\varphi = 32°$, where φ was controlled to satisfy $L\sin\varphi > h$¿

, so that liquids within the surface were emptied by gravity exceeding the capillary height. Initially, the surface was repellent with high droplet mobility. However, after filling the channels with liquid via a reservoir, the surface switched to a hemiwicking state, where liquid added to the surface was sucked into the structures. Once the liquid height reached a critical height, h ¿, the liquid in the channel was removed (between 16.47 s and 18.13 s), the surface transitioned back to the repellent state. This simple switching method for active control of the extreme surface wetting states not only provides versatile choices of liquid-surface material combinations, but also is advantageous over previously reported switching mechanisms based on complex coatings and external stimuli, which have inherent limitations such as biocompatibility or durability.[1, 9] More notably, controlled switching between such two extreme wetting states, i.e., repellency with mobile droplets to wicking, had not been achieved before with most other methods.[15]

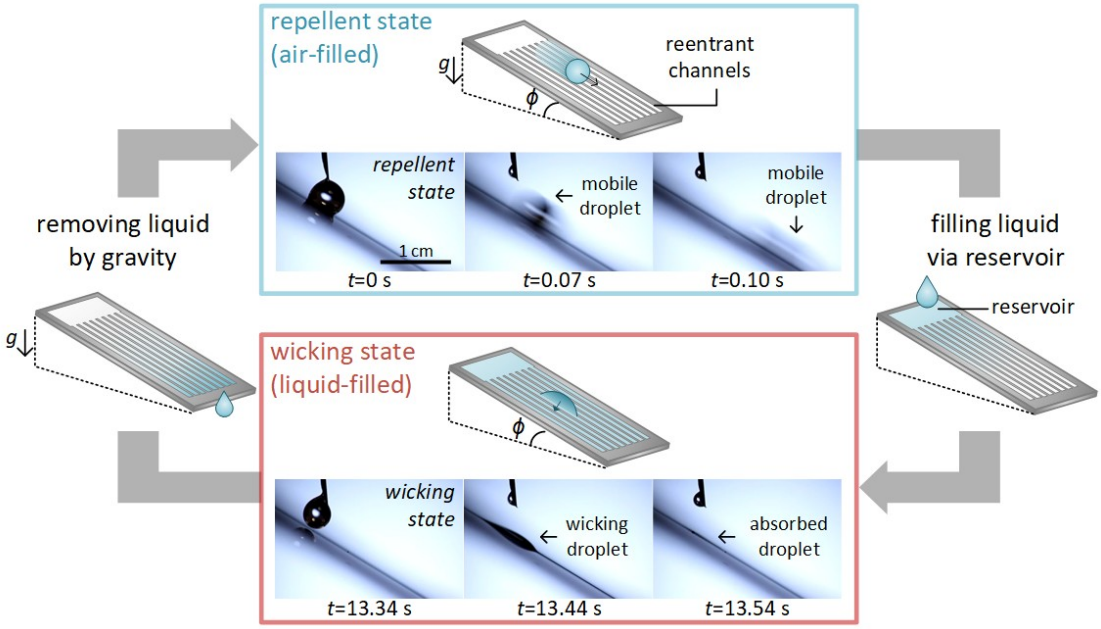

Figure 3. Switchable wettability of reentrant surfaces. Schematic of switching mechanisms and time-lapse images of active switching of wettability. Blue and red indicate the repellent and wicking wetting states, respectively. In the repellent state, the channels were filled with air, and a droplet that contacted the surface was repelled and was therefore highly mobile, rolling down the tilted surface. Then, by adding liquid to the channels via a pump at the reservoir, the surface was switched to a highly wetting state that absorbed liquid contacting the surface. Because the surface was tilted, as droplets were wicked into the surface and as

additional liquid was added from the reservoir, the channel continued to fill and eventually surpassed the sustainable capillary height of the channel, causing gravity to naturally empty the channel. This reverted the surface back to the repellent state.

Finally, we show the same strategy to tailor wetting behavior independent of intrinsic wettability also applies to liquid-liquid systems, where one typical application is oil-water separation. As opposed to conventional selective surfaces, the reentrant-surface-based approach does not need complex chemical coatings to determine selectivity; instead, the Laplace pressure of liquids are tailored by infusing reentrant structures with a desired liquid. Such functionality has been demonstrated on micropost arrays with a small reentrance angle α of 14°, which limited selectivity to liquids with intrinsic contact near 90° (72 and 83° degrees demonstrated)[27]. In this work, with reentrant channels without the C_4F_8 coating, i.e., a simple silicon and silicon dioxide surface, we showed that the intrinsic contact angle for selectivity can be extended to more extreme contact angles, where contact angles from 25.4° up to 150° were demonstrated using hexane in a water environment and vice versa. Furthermore, previous works only demonstrated the ability to tailor the repellent state. The additional understanding of dual Laplace pressures developed in this work also enabled the demonstration of control over hemiwicking selectivity as well. For the ease of visualization, the hexane droplets in a water environment were dyed yellow and the water droplets in a hexane environment were dyed blue. The wettability was measured by adding a liquid droplet to the surface immersed in the other liquid using a syringe. In a water environment, the surface wettability to hexane can be made either wetting or repellent by controlling the infused liquids in reentrant structures, i.e., wetting when infused with hexane (Figure 4a) and repelling when infused with water (Figure 4b). Similar behaviors were achieved for water in a hexane environment, i.e., wetting when infused with water (Figure 4c) and repelling when infused with hexane (Figure 4d). The apparent contact angles of the four cases are plotted in

Figure 4e as a function of intrinsic wettability ($\cos\theta$), which shows good agreement with the Cassie-Baxter and hemiwicking relations (see Section S3 of Supporting Information for description of wetting relations). Therefore, we demonstrated that by prefilling the surface with one liquid or the other, selective repellency or wetting of either liquid can be set as desired.

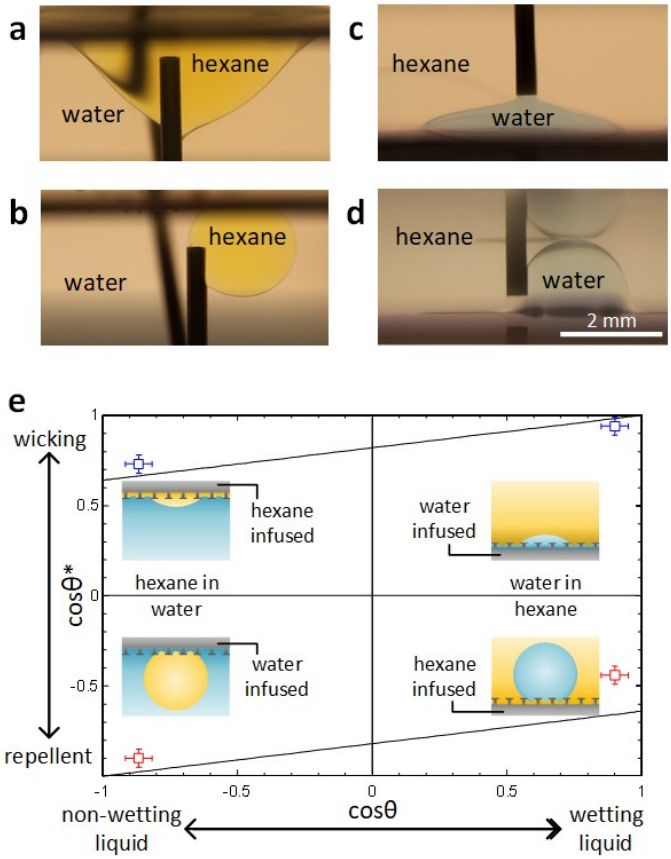

Figure 4. Selective wettability of reentrant surfaces demonstrated with hexane and water. In a water environment, the reentrant surfaces infused with hexane (a) wicks a hexane droplet (dyed yellow) while the surfaces infused with water (b) repels the hexane droplet. The same principles work in the hexane environment. The surfaces infused with water (c) wicks a water droplet (dyed blue) while the ones infused with hexane (d) repels the water droplet. (e) Experimental measurements of cosine of apparent contact angles with respect to cosine of intrinsic contact angle for the four selective wetting cases. Experimental data (blue: wicking, red: repelling) agree well with theoretical predictions (black lines). Schematics in Figure 4e are associated with photos of Figure 4a-d.

In conclusion, we demonstrated the dual Laplace pressures of reentrant features by capillary rise and dip tests, where the same reentrant surface could either maintain a liquid

within the structure or prevent the liquid from entering the structure against gravity by exhibiting negative or positive Laplace pressure. The reentrant structures were shown to enhance the Laplace pressure significantly, which is the driving force for wicking and repellency. Moreover, we showed by combining both positive and negative Laplace pressures on a single reentrant surface, the capillary height can be doubled, which could further impact wicking performance. We then demonstrated switchability and selectivity of a single reentrant surface by harnessing the dual Laplace pressure. We could actively switch the surface wettability from repellent to wicking, and vice versa, by simply prefilling or removing a liquid. Similarly, by prefilling a desired liquid within the reentrant structures, the surface could exhibit selective repellency or wetting of one liquid to the other. Since this switching and selective wetting mechanism does not require complex chemical modifications, it shows great potential for surface applications that previously have been limited by chemical compatibility, slow switching speed, external stimuli, or insignificant wettability change.

Experimental Section

Fabrication of Surfaces: The fabrication procedure of both normal and reentrant channels is depicted in Figure S3. A 2.5 μm layer of photoresist (Microposit S1822) was spin coated on polished silicon wafers that had a 1 μm thick silicon dioxide layer on the surface. The photoresist was exposed using an MLA150 Maskless Aligner. The resist was developed for 120 seconds in Microposit MF CD26 developer. The silicon dioxide was first etched using CF_4 (MPX/LPX RIE, STS). Then, the channels were etched in the silicon with deep reactive ion etching (Rapier DRIE, SPTS). For normal channels, the silicon dioxide was removed by placing the samples in 7:1 buffered oxide etch solution for 10 minutes. An isotropic SF_6 etch (Rapier DRIE, SPTS) was used to remove silicon below the silicon dioxide to create the reentrant geometry. A conformal, 60 nm thick hydrophobic polymer (C_4F_8) was deposited

(Rapier DRIE, SPTS). This allowed a large range of intrinsic contact angles to be tested and also created surfaces with uniform and consistent wettability.

Capillary Height Measurements: A custom-built experimental setup was used to measure the capillary height for each sample (Figure S10b). The samples were attached to a linear stage with a Vernier scale. This allowed the surfaces to be dipped into or withdrawn from a large pool of liquid. The Vernier scale (accurate to 1/100th of an inch) was used to determine the capillary height. In order to test the repellent state of reentrant surfaces, the initially dry surface was lowered into the liquid. A camera recorded the surface as it was lowered into the liquid. When the maximum negative capillary height into the liquid was exceeded, liquid entered the structures. The height at which this occurred was recorded. Similarly, to test the hemiwicking state of reentrant surfaces, the surfaces were prefilled with the liquid to be tested. The surface was then withdrawn from the pool of liquid. When the maximum positive capillary height of the liquid was exceeded, air entered the structures and the liquid receded. The height at which this occurred was recorded.

Prefilling Surface Structures: Prefilling the reentrant channels with liquid was achieved using a variety of methods. For naturally wicking liquids, the liquid was added to one end of the channels and in turn, filled the channels spontaneously. For ethanol/water mixtures that were not wicking, the channels were first filled with pure ethanol. Next, the ethanol filled sample was placed in a large container of the ethanol/water mixture to be tested. The pure ethanol within the surface structures was allowed to diffuse into the mixture, thereby replacing the ethanol in the channels with the mixture. Note that the volume of ethanol in the channels was on the order of ten microliters, whereas the container was more than one thousand times this size. Therefore, this filling method did not affect the final concentration of the mixture. Samples were then removed from the mixture such that the channels remained filled to conduct contact angle or capillary height measurements.

Switching Between Wicking and Repelling Experiments: To demonstrate the ability to switch between states, the reentrant channels were tilted at an angle of 30°. The surface was initially dry. Therefore, when a syringe added a liquid mixture of 83% water and 17% ethanol to the surface, a droplet was formed in the Cassie state and thereby repelled. However, by adding the liquid to the channels using a pump at the reservoir, a droplet added to the surface formed the hemiwicking state and was wicked into the surface structures. When enough liquid was added to the tilted surface, hydrostatic pressure from gravity caused the liquid within the structure to spontaneously dewet from the channel, thereby recovering the state filled with air. As such, the repellent Cassie state was recovered. This process was continuously repeated multiple times in Movie S4.

Selective Wicking and Repellency Experiments: The measurement was done with the same setup for the contact angle measurement. Two immiscible liquids, water and hexane, were used for testing. First, a drop of one of two liquids was placed on a flat surface while the entire surface was submerged in the other liquid to confirm the intrinsic contact angle, θ. Then, the selective wicking was achieved by infusing the same liquid as the droplet into the reentrant structures. On the other hand, the repellency was achieved by infusing the other liquid into the reentrant structures. In the case of testing the wettability of hexane within a water environment, due to the density difference of two liquids, the surface was flipped upside-down, and a syringe was placed under the surface to add a hexane droplet.

Supporting Information

Supporting Information is available from the Wiley Online Library or from the author.

Acknowledgements

K.L.W. and Y.S. contributed equally to this work. This work was performed in part at the Center for Nanoscale Systems (CNS), a member of the National Nanotechnology Infrastructure Network (NNIN), which is supported by the National Science Foundation under NSF award no. 1541959. CNS is part of Harvard University. We gratefully acknowledge the technical support from the NanoStructures Laboratory and Microsystems Technology

Laboratories at MIT. This work was supported by the Cooperative Agreement between the Masdar Institute of Science and Technology (Masdar Institute), Abu Dhabi, UAE and the Massachusetts Institute of Technology (MIT), Cambridge, MA, USA - Reference 02/MI/MIT/CP/11/07633/GEN/G/00. Y.S. acknowledges that the information, data, or work presented herein was funded in part by the Advanced Research Projects Agency-Energy (ARPA-E), U. S. Department of Energy, under Award Number DE-AR0000ABC. Z.L. acknowledges funding support from the Air Force Office of Scientific Research with Dr. Ali Sayir as program manager.

Conflict of Interest

A patent has been filed on this work (US 2020/0368778 A1).

Received: ((will be filled in by the editorial staff))
Revised: ((will be filled in by the editorial staff))
Published online: ((will be filled in by the editorial staff))

REFERENCES

[1] a) G. Kwon, E. Post, A. Tuteja, *MRS Communications* **2015**, *5*, 475; b) J.-J. Li, Y.-N. Zhou, Z.-H. Luo, *Prog. Polym. Sci.* **2018**, *87*, 1.

[2] a) P. Comanns, G. Buchberger, A. Buchsbaum, R. Baumgartner, A. Kogler, S. Bauer, W. Baumgartner, *J. R. Soc. Interface* **2015**, *12*, 20150415; b) C. K. Camplisson, K. M. Schilling, W. L. Pedrotti, H. A. Stone, A. W. Martinez, *Lab. Chip* **2015**, *15*, 4461; c) Y. Zhu, D. S. Antao, R. Xiao, E. N. Wang, *Adv. Mater.* **2014**, *26*, 6442.

[3] R. Wang, K. Hashimoto, A. Fujishima, M. Chikuni, E. Kojima, A. Kitamura, M. Shimohigoshi, T. Watanabe, *Nature* **1997**, *388*, 431.

[4] a) J. Yang, Z. Zhang, X. Xu, X. Zhu, X. Men, X. Zhou, *J. Mater. Chem.* **2012**, *22*, 2834; b) L. Feng, Z. Zhang, Z. Mai, Y. Ma, B. Liu, L. Jiang, D. Zhu, *Angew. Chem. Int. Ed.* **2004**, *43*, 2012.

[5] a) Y. Zhu, D. S. Antao, Z. Lu, S. Somasundaram, T. Zhang, E. N. Wang, *Langmuir* **2016**, *32*, 1920; b) A. Faghri, *Heat pipe science and technology*, Taylor & Francis, Washington, DC **1995**.

[6] L. Dong, A. K. Agarwal, D. J. Beebe, H. Jiang, *Nature* **2006**, *442*, 551.

[7] F. Rios, S. N. Smirnov, *Chem. Mater.* **2011**, *23*, 3601.

[8] a) G. Caputo, C. Nobile, T. Kipp, L. Blasi, V. Grillo, E. Carlino, L. Manna, R. Cingolani, P. D. Cozzoli, A. Athanassiou, *The Journal of Physical Chemistry C* **2008**, *112*, 701; b) G. Zhang, X. Zhu, F. Miao, D. Tian, H. Li, *Organic & Biomolecular Chemistry* **2012**, *10*, 3185.

[9] K. Riehemann, S. W. Schneider, T. A. Luger, B. Godin, M. Ferrari, H. Fuchs, *Angew. Chem. Int. Ed.* **2009**, *48*, 872.

[10] Y. Chen, N. Doshi, B. Goldberg, H. Wang, R. J. Wood, *Nat. Commun.* **2018**, *9*, 2495.

[11] D. Quéré, *Annual Review of Materials Research* **2008**, *38*, 71.

[12] a) Liang, X. Feng, J. Liu, P. C. Rieke, G. E. Fryxell, *Macromolecules* **1998**, *31*, 7845; b) S. S. Chhatre, A. Tuteja, W. Choi, A. Revaux, D. Smith, J. M. Mabry, G. H. McKinley, R. E. Cohen, *Langmuir* **2009**, *25*, 13625.

[13] a) K. Ichimura, S.-K. Oh, M. Nakagawa, *Science* **2000**, *288*, 1624; b) X. Feng, L. Feng, M. Jin, J. Zhai, L. Jiang, D. Zhu, *J. Am. Chem. Soc.* **2004**, *126*, 62.

[14] a) F. Xia, H. Ge, Y. Hou, T. Sun, L. Chen, G. Zhang, L. Jiang, *Adv. Mater.* **2007**, *19*, 2520; b) M. A. Frysali, S. H. Anastasiadis, *Langmuir* **2017**, *33*, 9106.
[15] a) J. Lahann, S. Mitragotri, T.-N. Tran, H. Kaido, J. Sundaram, I. S. Choi, S. Hoffer, G. A. Somorjai, R. Langer, *Science* **2003**, *299*, 371; b) A. Ahuja, J. A. Taylor, V. Lifton, A. A. Sidorenko, T. R. Salamon, E. J. Lobaton, P. Kolodner, T. N. Krupenkin, *Langmuir* **2008**, *24*, 9.
[16] J. Yong, S. C. Singh, Z. Zhan, F. Chen, C. Guo, *ACS Appl. Mater. Interfaces* **2019**, *11*, 8667.
[17] a) J. Zhang, X. Lu, W. Huang, Y. Han, *Macromol. Rapid Commun.* **2005**, *26*, 477; b) W. Choi, A. Tuteja, S. Chhatre, J. M. Mabry, R. E. Cohen, G. H. McKinley, *Adv. Mater.* **2009**, *21*, 2190.
[18] S. Wang, Y. Song, L. Jiang, *Nanotechnology* **2006**, *18*, 015103.
[19] a) A. Tuteja, W. Choi, M. Ma, J. M. Mabry, S. A. Mazzella, G. C. Rutledge, G. H. McKinley, R. E. Cohen, *Science* **2007**, *318*, 1618; b) A. K. Kota, G. Kwon, W. Choi, J. M. Mabry, A. Tuteja, *Nat. Commun.* **2012**, *3*, 1025.
[20] a) Q. Wang, Z. Cui, Y. Xiao, Q. Chen, *Appl. Surf. Sci.* **2007**, *253*, 9054; b) J. Zhang, S. Seeger, *Adv. Funct. Mater.* **2011**, *21*, 4699.
[21] a) B. Wang, Z. Guo, *Appl. Phys. Lett.* **2013**, *103*, 063704; b) C. Wang, T. Yao, J. Wu, C. Ma, Z. Fan, Z. Wang, Y. Cheng, Q. Lin, B. Yang, *ACS Appl. Mater. Interfaces* **2009**, *1*, 2613; c) J. Li, L. Shi, Y. Chen, Y. Zhang, Z. Guo, B.-l. Su, W. Liu, *J. Mater. Chem.* **2012**, *22*, 9774.
[22] N. Liu, Y. Cao, X. Lin, Y. Chen, L. Feng, Y. Wei, *ACS Appl. Mater. Interfaces* **2014**, *6*, 12821.
[23] J.-B. Fan, Y. Song, S. Wang, J. Meng, G. Yang, X. Guo, L. Feng, L. Jiang, *Adv. Funct. Mater.* **2015**, *25*, 5368.
[24] a) T. L. Liu, C.-J. C. Kim, *Science* **2014**, *346*, 1096; b) K. L. Wilke, D. J. Preston, Z. Lu, E. N. Wang, *ACS Nano* **2018**, *12*, 11013.
[25] K. L. Wilke, Z. Lu, Y. Song, E. N. Wang, *Proceedings of the National Academy of Sciences* **2022**, *119*, e2109052119.
[26] a) K. L. Wilke, K. B. Kalinina, Y. Zhu, D. J. Preston, D. S. Antao, S. Adera, E. N. Wang, presented at *International Heat Transfer Conference*, Beijing, China, August 10-15, 2018, **2018**; b) T. Liu, C. Kim, presented at *28th IEEE International Conference on Micro Electro Mechanical Systems (MEMS)*, 18-22 Jan., **2015**.
[27] X. Tian, V. Jokinen, J. Li, J. Sainio, R. H. A. Ras, *Adv. Mater.* **2016**, *28*, 10652.

The dual Laplace pressure of reentrant structures is demonstrated by capillary rise/dip tests with reentrant microchannels, which enables tailoring the surface wetting state to either repellent or hemiwicking state regardless of intrinsic wettability. Furthermore, functionalities such as switchability and selectivity are achieved by harnessing the dual Laplace pressure. This work has important implications in enabling extreme wettabilities by surface structures alone.

Keyword: reentrant structures, wettability, switchability, liquid separation, smart surfaces, functional surfaces

K. L. Wilke, Y. Song, Z. Lu, E. N. Wang*

Enhanced Laplace Pressures for Functional Surfaces: Switchability and Selectivity